On the temperature sensing capability of a fibre optic SPR mechanism based on bimetallic alloy nanoparticles

2009 J. Phys. D: Appl. Phys. 42 045104

(http://iopscience.iop.org/0022-3727/42/4/045104)

IOP PUBLISHING JOURNAL OF PHYSICS D: APPLIED PHYSICS

J. Phys. D: Appl. Phys. **42** (2009) 045104 (7pp) doi:10.1088/0022-3727/42/4/045104

On the temperature sensing capability of a fibre optic SPR mechanism based on bimetallic alloy nanoparticles

Anuj K Sharma[1], Himansu S Pattanaik[2] and Gerhard J Mohr[1]

[1] Institute of Physical Chemistry, Friedrich-Schiller University, Lessingstraße 10, 07743 Jena, Germany
[2] Private address, Orlando, FL, USA

E-mail: anuj.sharma@uni-jena.de and hpattana@creol.ucf.edu

Received 4 July 2008, in final form 29 September 2008
Published 15 January 2009
Online at stacks.iop.org/JPhysD/42/045104

Abstract

In this work, we have investigated the capability of different bimetallic nanoparticle alloy combinations to be used in fibre optic temperature sensing based on the technique of surface plasmon resonance (SPR). The metals considered for the present analysis are silver, gold and aluminium. The analysis is derived mainly from the thermo-optic effect along with some fundamental concepts of metal optics such as surface scattering, phonon–electron scattering and electron–electron scattering. The performance of the sensor with three different bimetallic nanoparticle alloy combinations is evaluated and compared, numerically, in terms of its sensitivity and accuracy. On the basis of the comparison and some logistic criterion, we predict the best possible bimetallic alloy combination along with a requisite alloy composition ratio that simultaneously provides higher values of both sensitivity and accuracy which is not possible with any single metallic nanoparticle layer.

1. Introduction

The optical phenomenon of surface plasmon resonance (SPR) has been widely used for a fast and precise detection of several physical, chemical and bio-chemical parameters in the last two decades [1–4]. In the Kretschmann SPR technique [5], when a p-polarized electromagnetic wave, namely, surface plasmon wave (SPW), supported at a metal–dielectric interface is coupled with an evanescent wave of the same propagation constant, strong absorption of light takes place. Due to this absorption, the output signal demonstrates a sharp dip at a particular wavelength known as the resonance wavelength. The resonance condition is given by the following expression:

$$K_0 n_c \sin\theta = \mathrm{Re}\left[K_0\left(\frac{\varepsilon_m \varepsilon_s}{\varepsilon_m + \varepsilon_s}\right)^{1/2}\right]; \qquad K_0 = \frac{2\pi}{\lambda}. \quad (1)$$

The term on the left-hand side is the evanescent wave propagation constant (K_{ev}) generated due to attenuated total reflection (ATR) of the light incident at an angle θ through a light coupling device (such as prism or optical fibre) of the refractive index n_c. The right-hand term is the real part of the SPW propagation constant (K_{SP}) with ε_m as the metal–dielectric constant and ε_s as the dielectric constant of the sensing (dielectric) layer. In the case of metal nanoparticles, the term ε_m is dependent on the size, shape and distribution of nanoparticles. Depending upon the combination of metal and dielectric media, the resonance condition may be satisfied at different wavelengths due to all the media involved being dispersive in nature. Apart from material dispersion, the thermo-optic effect among the metal and dielectric media may also significantly affect the above resonance condition. In fact, this aspect related to the thermo-optic effect may even be exploited to design an SPR based temperature sensor. A few models have already been proposed for SPR based temperature sensing [6, 7]. However, none of them has utilized the concept of bimetallic alloy nanoparticles. It has been shown in a previous study that fibre optic SPR refractive index sensors with different bimetallic alloy nanoparticles are able to show a balanced sensing performance by efficiently minimizing the usual trade-off between the sensitivity and the accuracy of an SPR sensor [8]. In this work, we have theoretically analysed the SPR sensing capabilities of different bimetallic alloy nanoparticle combinations made out of three metals: Ag, Au and Al. The analysis is carried out separately for all three bimetallic alloy combinations and a comparison in terms

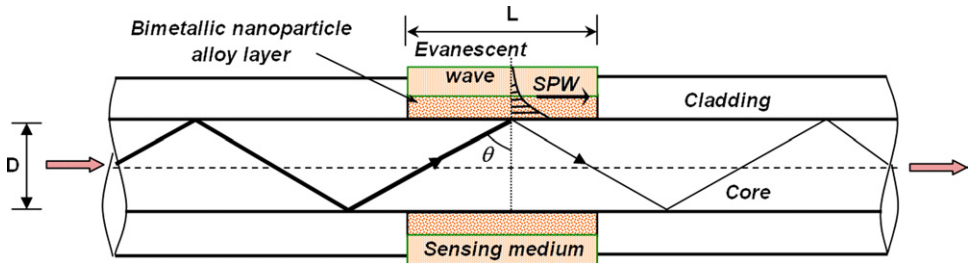

Figure 1. A fibre optic SPR sensor with bimetallic nanoparticle alloy layers.
(This figure is in colour only in the electronic version)

of their sensitivity and accuracy is carried out to predict the conditions for the best sensing performance. The wavelength interrogation method in combination with an optical fibre is used for the analysis. Finally, the most suitable bimetallic alloy combination is predicted in order to provide simultaneously high values for both the performance parameters in the context of reference temperature detection.

2. Theoretical model

The ATR method with the Kretschmann configuration is employed. A step index multimode silica fibre is considered in which a small length of the cladding is removed from the middle portion of the fibre in order to access the evanescent field. The unclad portion of the fibre is coated with a bimetallic alloy nanoparticle film. This is further surrounded by the liquid sensing layer (figure 1). Light is launched into one end of the fibre through a broadband light source with proper optics. The other end is connected to a detection system to record the output signal.

For the present analysis, the central core of the optical fibre is assumed to be made of silica. Ghosh *et al* modelled the temperature dependence of the dielectric constant of silica [9]:

$$\varepsilon_{\text{silica}}(\lambda, T) = 1.315\,52 + (0.690\,754 \times 10^{-5})T + \frac{(0.788\,404 + T \times 0.235\,835 \times 10^{-4})\lambda^2}{\lambda^2 - (0.011\,0199 + T \times 0.584\,758 \times 10^{-6})} + \frac{(0.913\,16 + T \times 0.548\,368 \times 10^{-6})\lambda^2}{\lambda^2 - 100}. \quad (2)$$

The wavelength and temperature dependent dielectric constant of any metal can be appropriately represented by the Drude formula:

$$\varepsilon_{\text{m}}(\lambda, T) = 1 - \frac{\lambda^2}{\lambda_{\text{p}}^2(T)\left(1 + \text{i}\dfrac{\lambda}{\lambda_{\text{c}}(T)}\right)}, \quad (3)$$

where λ_{p} and λ_{c} denote the plasma wavelength and the collision wavelength, respectively. The origin of the temperature dependence of the plasma wavelength (λ_{p}) is the temperature dependence of the density and the effective mass of electrons. If T is the operating temperature, the temperature dependent plasma oscillation wavelength is given by [10]

$$\frac{1}{\lambda_{\text{p}}(T)} = \frac{1}{\lambda_{\text{p0}}}[1 + 3\gamma_{\text{m}}(T - T_0)]^{-1/2}, \quad (4)$$

where γ_{m} is the thermal linear expansion coefficient of the metal and T_0 is the room temperature which acts as the reference temperature. λ_{p0} is the plasma frequency of the metal at room temperature. The collision wavelength is also dependent on temperature and is described as [11–14]

$$\frac{1}{\lambda_{\text{c}}(T, R_{\text{particle}})} = \frac{2\pi c\varepsilon_0}{\lambda_{\text{p}}^2\sigma(0)} \frac{\left[\dfrac{1}{10} + \left(\dfrac{T}{T_{\text{D}}}\right)^5 \displaystyle\int_0^{T_{\text{D}}/T} \frac{z^4}{(\text{e}^z - 1)}\,\text{d}z\right]}{\displaystyle\int_0^1 \frac{z^5}{(\text{e}^z - 1)(1 - \text{e}^{-z})}\text{d}z} + \frac{\pi^3\Gamma\Delta}{12chE_{\text{F}}}\left[(k_{\text{B}}T)^2 + \left(\frac{h\omega}{4\pi^2}\right)^2\right] + \frac{v_{\text{f}}}{2\pi c R_{\text{particle}}}. \quad (5)$$

The first term in the above expression corresponds to the wavelength of phonon–electron scattering and the second term is associated with the wavelength of electron–electron scattering. The third term is due to the nanoparticle-size effect (i.e. surface scattering), when the particle size becomes smaller than the mean free path of the electrons. The values and notation of the parameters concerning equation (5) are given in table 1 [10–14]. The average dielectric constant (ε_{A}) of the bimetallic alloy could be assumed to vary with the composition-weighted average of the dielectric constants (say, ε_{m1} and ε_{m2}) of the two metals and is given by [15]

$$\varepsilon_{\text{A}}(x, \lambda, T) = x\varepsilon_{\text{m1}}(\lambda, T) + (1 - x)\varepsilon_{\text{m2}}(\lambda, T), \quad (6)$$

where x is the volume fraction (or alloy fraction or composition ratio) of the nanoparticles of the first metal.

Such bimetallic alloys do exist and their fabrication and optical properties have been investigated in much detail. In general, the alloy film is generally made of either many thin layers of two metals (i.e. multilayered methodology) or by mixing the nanoparticles of two metals in the desired proportions. For instance, the preparation along with optical properties of Ag–Al [16] and Au–Al [17] alloys with ultrahigh vacuum for the film evaporation method and Ag–Au alloys with sequential sputtering [15] and co-reduction of chloroauric acid ($HAuCl_4$) and silver nitrate ($AgNO_3$) with sodium citrate [18] have been reported. However, in all the above methods, the dielectric constant of the bimetallic alloy film depends on the composition-weighted average of the dielectric constants according to equation (6).

Furthermore, as far as the dielectric sensing medium is concerned, it has to be of a reasonably high thermo-optic

Table 1. Metal parameters used for the numerical simulations.

Parameter	Ag	Au	Al
λ_{p0} (m)	1.4541×10^{-7}	1.6826×10^{-7}	1.0657×10^{-7}
γ_m (K^{-1})	1.89×10^{-5}	1.42×10^{-5}	2.40×10^{-5}
Debye temperature, T_D (K)	215	170	396
Fermi energy, E_F (eV)	5.48	5.53	11.7
dc resistivity, $1/\sigma(0)$ (Ω cm)	1.16×10^{-6}	1.32×10^{-6}	3.90×10^{-6}
Fractional umklapp scattering, Δ	0.73	0.77	0.75
Average scattering probability, Γ	0.55	0.55	0.52
Fermi velocity, v_f ($m\,s^{-1}$)	1.40×10^6	1.40×10^6	2.02×10^6

coefficient (such as titanium oxide or silicone acrylate) for efficient temperature sensing with SPR. However, the family of the above-mentioned polymers exhibits strong absorption in the ultraviolet (UV) wavelength range and SPR excitation in the UV range may cause the solarization effect in optical fibres. The solarization effect can not only disturb the modal properties of the fibre but also adversely affect the sensing performance. Therefore, we have considered water as the active sensing layer in this study. The SPR excitation for water takes place in the visible range. Also, the refractive index of water is very sensitive to temperature variations. The wavelength, density and temperature dependent refractive index of water according to the Lorentz–Lorentz relation derived by Scheibener *et al* [19] is as follows:

$$\left(\frac{n_s^2-1}{n_s^2-1}\right)\frac{1}{\rho^*} = a_0 + a_1\rho^* + a_2T^* + a_3\lambda^{*2}T^* + \frac{a_4}{\lambda^{*2}} + \frac{a_5}{\lambda^{*2}-\lambda_{UV}^2} + \frac{a_6}{\lambda^{*2}-\lambda_{IR}^2} + a_7\rho^{*2}, \quad (7)$$

where $\rho^* = \rho/\rho_0$; $\rho_0 = 1000\,kg\,m^{-3}$; $\lambda^* = \lambda/\lambda_0$; $\lambda_0 = 0.589\,\mu m$; $T^* = T/T_0$; $T_0 = 273.15\,K$.

In the above equation, ρ is the density (in $kg\,m^{-3}$), λ is the wavelength of the light (in μm) and T is the operating temperature (in K). Furthermore, in order to obtain the expression for the intensity reflection coefficient (R) for the p-polarized incident beam we have used the matrix method for a fibre core–metal layer-sensing medium multilayer system [8]. The matrix method takes into account the wavelength and temperature dependent dielectric constants of all the media involved in order to calculate R. Finally, the normalized output power (P_{trans}) transmitted at the output end of the fibre is calculated for all guided rays launching as we carried out in our previous study for the bimetallic alloy nanoparticle based fibre optic SPR sensor [8].

3. Performance parameters

The performance of the SPR-based temperature sensor is mainly evaluated in terms of two performance parameters, namely, sensitivity and accuracy. Sensitivity depends on the amount of shift in the resonance wavelength (λ_{res}) for a given range of temperature under detection. More precisely, the sensitivity (S_T) corresponds to the shift in the resonance wavelength ($\delta\lambda_{res}$) for a unit change in temperature (δT), i.e.

$$S_T = \frac{\delta\lambda_{res}}{\delta T}. \quad (8)$$

The above definition suggests that the shift in the resonance wavelength corresponding to any temperature range should be as large as possible for highly sensitive temperature detection. Furthermore, the accuracy of temperature detection depends on the spectral width of the SPR curve ($\delta\lambda_{SW}$). The broader the SPR curve, the greater will be the error in recording the exact resonance wavelength, which amounts to more error in temperature detection. Therefore, the SPR curve width should be as small as possible for greater accuracy of temperature detection. Hence, the accuracy (A_T) of an SPR-based temperature sensor depending upon the SPR curve width and detector's resolution can be defined as

$$A_T = \frac{\delta\lambda_{DR}}{\delta\lambda_{SW}}. \quad (9)$$

In the above equation, $\delta\lambda_{DR}$ is the resolution of the detector. At present, the generally used detectors have a spectral resolution ($\delta\lambda_{DR}$) of 0.01 nm, which is also taken in the present analysis.

4. Results and discussion

Figure 2 depicts the simulated SPR transmittance curves (P_{trans} versus λ) corresponding to the fibre optic SPR sensor with a nanoparticle alloy layer for three different bimetallic combinations, namely, Ag–Au, Ag–Al and Au–Al. For a preliminary indication of the sensitivity and accuracy of the temperature sensor, the SPR curves are plotted for two temperatures (i.e. $T = 300$ and 301 K) for each bimetallic combination. In all these combinations, the alloy composition ratio (x) is taken as 0.5. The values of other fibre parameters are numerical aperture (NA) = 0.24, fibre core diameter (D) = 600 μm, sensing region length (L) = 15 mm and particle size ($R_{particle}$) = 8 nm. The thickness (d) of the whole layer of alloy nanoparticles is taken as 50 nm. It is apparent from figure 2 that the bimetallic combinations are able to tune the position as well as the width of the SPR curve depending upon which two metals are coupled. Moreover, the shift in the resonance wavelength corresponding to two temperatures is different for all three bimetallic alloy combinations. More precisely, the resonance wavelength shifts by 1.90 nm for Ag–Au (i.e. from 534.91 to 533.01 nm), 0.87 nm for Au–Al (i.e. from 449.27 to 448.40 nm) and 0.18 nm for Ag–Al (i.e. from 429.96 to 429.78 nm).

At this point, it is important to verify the correlation between the plasmon resonance condition (given in

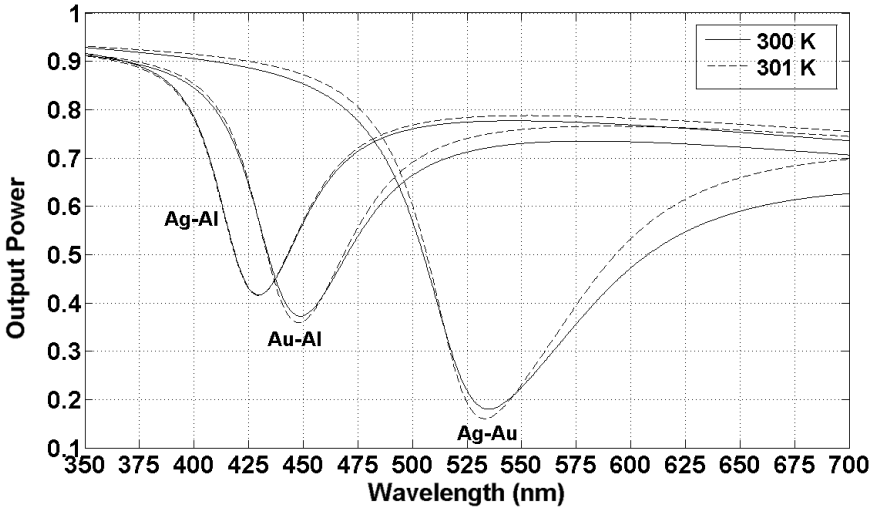

Figure 2. SPR transmittance curves for fibre optic temperature sensor corresponding to three different bimetallic nanoparticle alloy combinations at $T = 300$ and $T = 301$ K.

equation (1)) and the corresponding SPR curves we obtained in figure 2. For this purpose, we calculated the spectral variation of the propagation constants of the evanescent wave (K_{ev}) and of the SPW (K_{SP}) for all three bimetallic combinations at both temperatures. Figure 3(a) shows the corresponding variation of propagation constants at $T = 300$ K. As is visible, the matching of K_{ev} and K_{SP} occurs at 429.96 nm for Ag–Al (0.5), at 449.27 nm for Au–Al (0.5) and at 534.91 nm for Ag–Au (0.5). These values of resonance wavelengths for three alloy combinations at $T = 300$ K are in full accordance with the corresponding SPR curves shown in figure 2. Figure 3(b) shows the corresponding variation of propagation constants at $T = 301$ K. Similar to figure 3(a), it was observed that the values of resonance wavelengths for three alloy combinations at $T = 301$ K are also in full accordance with the corresponding SPR curves shown in figure 2. More precisely, at $T = 301$ K, the matching of K_{ev} and K_{SP} occurs at 429.78 nm for Ag–Al (0.5), at 448.40 nm for Au–Al (0.5) and at 533.01 nm for Ag–Au (0.5). Thus, figures 3(a) and (b) confirm the correlation of the resonance condition (equation (1)) with the SPR curves shown in figure 2.

Furthermore, the mean spectral width for individual SPR curves is found to be 85.06 nm for Ag–Au, 54.66 nm for Au–Al and 45.46 nm for Ag–Al. Hence, based on the above observations regarding the variation in position, shifting and spectral width of SPR curves for different bimetallic combinations, it is quite worthwhile to estimate and figure out the best combination of two metals which can provide the maximum sensitivity and the highest accuracy.

Figure 4 shows the variation of sensitivity with varying alloy composition ratios (x) for three bimetallic nanoparticle alloy combinations. As mentioned in the theoretical model as well, x is the volume fraction of the first metal. For instance, in the case of the Ag–Al alloy, when x is varied from 0 to 1 in figure 4, it means that it is the volume fraction of Ag nanoparticles. Accordingly, the volume fraction of Al nanoparticles will be $1 - x$ and the dielectric constant of the alloy nanoparticle layer will accordingly vary as per equation (6). Similarly, for the Au–Al alloy, x is the volume fraction of Au nanoparticles, and for the Ag–Au alloy, x is the volume fraction of Ag nanoparticles. More precisely, x is the volume fraction of the metal which is written first in an alloy combination. The curves are simulated for $\delta T = 0.5$ K (i.e. T changing from 300 to 300.5 K). The figure also contains the sensitivity of single metallic nanoparticle layers at points 0 and 1 on the x-axis and it clearly vindicates the above observation that the single Au layer provides the maximum sensitivity whereas the single Al layer provides the minimum sensitivity. As is visible, the Ag–Al combination provides minimum sensitivity for any ratio of their corresponding alloy compositions. Ag–Au alloy with $x < 0.65$ and Au–Al alloy with $x > 0.65$ provide higher sensitivity than their two counterparts. It suggests that the larger fraction of Au nanoparticles is better to attain higher sensitivity. Similarly, figure 5 shows the corresponding variation in accuracy with varying alloy composition ratios. As far as the single metal nanoparticle layers are concerned, it clearly suggests that the single Al layer provides the highest accuracy whereas the single Au layer provides the lowest accuracy. Among the three bimetallic combinations, Ag–Al is clearly better than the other two combinations. The Au–Al combination is second best to the Ag–Al alloy for most of the range of x-values. The Ag–Au combination provides minimum values of accuracy among all the cases for most of the values of the alloy composition ratio. This suggests that the larger fraction of Al nanoparticles is better to attain higher accuracy.

From the above results, it is clear that no single alloy combination of metal nanoparticles is able to provide improved values of both accuracy and sensitivity, simultaneously. The Ag–Al combination is the most accurate one but the least sensitive. The Au–Al and Ag–Au combinations are more sensitive but not highly accurate in comparison with Ag–Al. Since both accuracy and sensitivity should be as large as possible, we are inclined to find a unique value of the alloy composition ratio for every bimetallic combination around which satisfactory values of both accuracy and sensitivity can be achieved. For this purpose, we define a logical criterion that accuracy should not be less than 1.6×10^{-4} and sensitivity

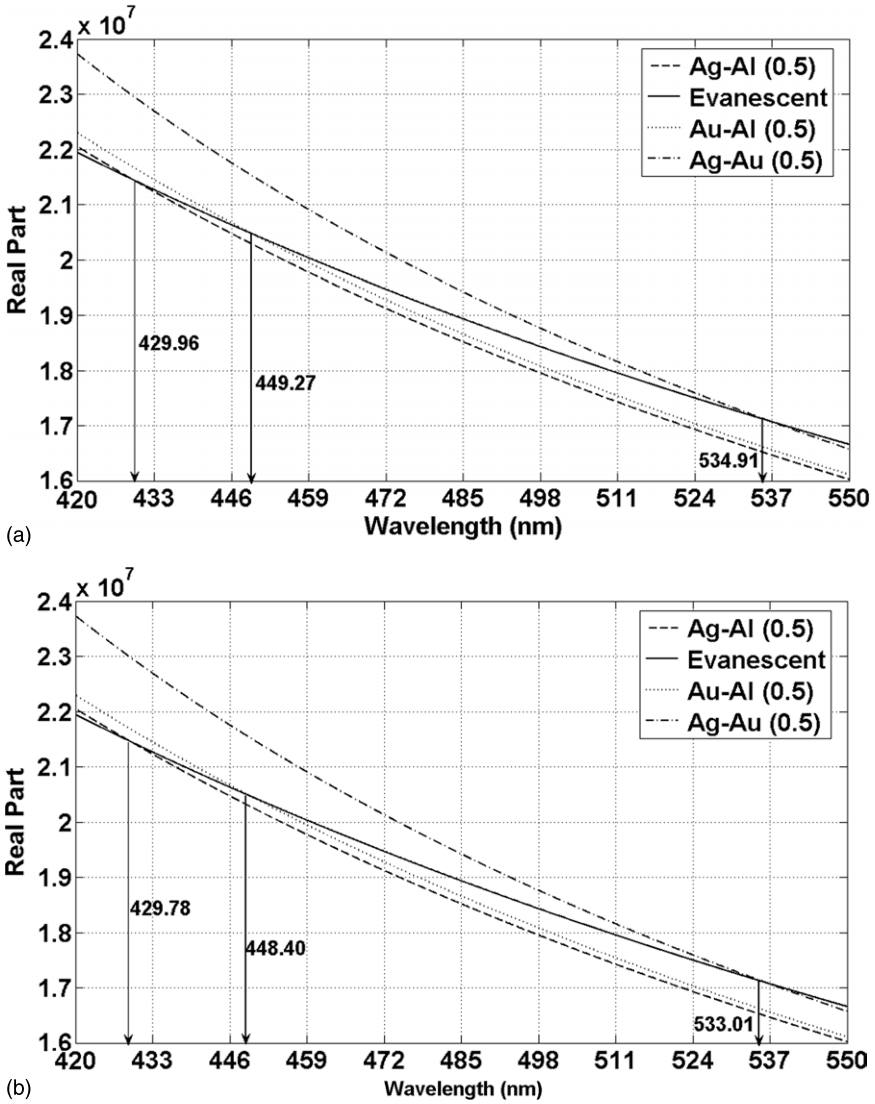

Figure 3. Spectral variation of propagation constants for the evanescent wave (K_{ev}) and the SPW (K_{SP}) for three bimetallic combinations (Ag–Al, Au–Al and Ag–Au) at (*a*) $T = 300$ and (*a*) $T = 301$ K. The results correspond to an alloy fraction (x) of 0.5.

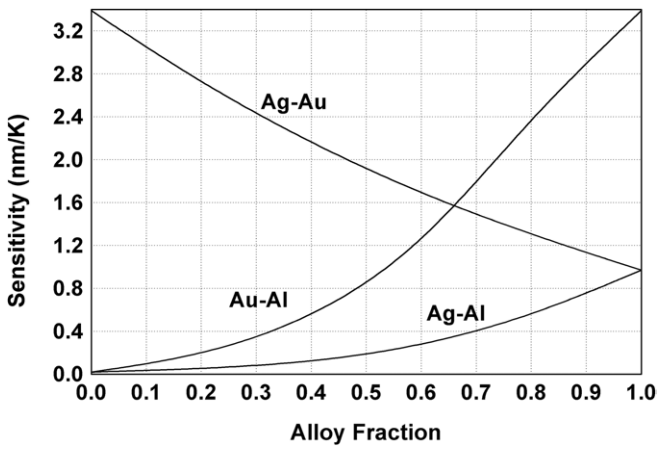

Figure 4. Variation of sensitivity (in nm K^{-1}) with the alloy fraction for three different bimetallic combinations. The temperature (T) is varied from 300 to 300.5 K, i.e. $\delta T = 0.5$ K.

should not be less than 1.6 nm K^{-1}. Both these criterion values of sensitivity and accuracy fall just below the middle of the respective variation ranges in figures 4 and 5, respectively. When we apply this criterion to all three combinations, we find that only Au–Al very nearly satisfies the above criterion with an alloy fraction of 0.65. The other two combinations Ag–Au and Ag–Al do not satisfy the above criterion for any value of alloy fraction. Hence, we can define two categories of bimetallic combinations on the basis of the above criterion. In the first category, Au–Al with an alloy fraction of nearly 0.65 can be classified as the best choice as it provides reasonably high values of both accuracy and sensitivity, simultaneously. In more general terms, the Au–Al alloy combination with x lying somewhere between 0.6 and 0.7 is able to provide a balanced set of both the performance parameters. In the second category, Ag–Al at around $x = 0.9$ is able to provide the requisite accuracy (1.6×10^{-4}) but at the cost of sensitivity, which becomes as small as 1.20 nm K^{-1}. Further, Ag–Au at around $x = 0.65$ shows a similar contrast to the requisite

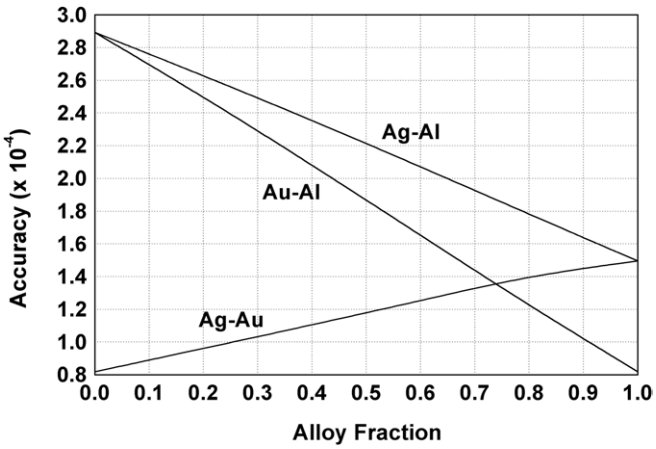

Figure 5. Variation of accuracy with the alloy fraction for three different bimetallic combinations. The temperature (T) is varied from 300 to 300.5 K, i.e. $\delta T = 0.5$ K.

sensitivity (1.6 nm K^{-1}) at the cost of accuracy, which gets as low as 1.3×10^{-4}.

Here, it is to be mentioned that all the above results correspond to the metal nanoparticle size (R_{particle}) of 8 nm. However, it has been shown in our previous studies on the Ag–Au bimetallic nanoparticle alloy based fibre optic SPR sensor that the nanoparticle size only affects the accuracy of the sensor whereas sensitivity remains almost unaffected [20]. In this study as well, it can be shown from equation (5) that the increase in the particle size leads to an increase in the collision wavelength followed by a fall in the imaginary (absorption) part of the surface plasmon propagation constant. Hence, absorption of light power is inversely proportional to the size of metal nanoparticles in the alloy film. Therefore, the transmitted power should decrease and the SPR curve should shift downwards with a decrease in the nanoparticle size, which further gives rise to broadening of the curve. Therefore, according to equation (9), the accuracy increases with an increase in the nanoparticle size for any value of T. Furthermore, it was shown in the previous study [20] that the position of the SPR dip at the wavelength scale remained almost the same for all the particle sizes. Hence, the sensitivity of the sensor is almost independent of the size of the metal nanoparticle. This suggests that the performance of the present temperature sensing scheme based on bimetallic nanoparticle alloys can be further improved in terms of its accuracy by taking a larger size of nanoparticles.

5. Conclusions

In conclusion, a detailed theoretical model for the SPR-based temperature sensor with a bimetallic alloy nanoparticle layer and an optical fibre is proposed. On the basis of the detailed theoretical analysis related to the above sensor, it is found that no single metal nanoparticle coating (among Ag, Au and Al) is able to provide reasonable values for the two main performance parameters, i.e. sensitivity and accuracy, simultaneously. However, when the nanoparticles of these metals are used in bimetallic combinations of well-defined alloy fractions, one can find an overall sensing performance with high sensitivity and high accuracy. The proposed bimetallic alloy combinations were classified into two categories based on a logical criterion. The Au–Al alloy combination with an alloy fraction in the vicinity of 0.65 is able to show significantly high values of sensitivity and accuracy, simultaneously. The Ag–Au and Ag–Al combinations show inferior overall performance in comparison with the Au–Al alloy.

Acknowledgment

Anuj Kumar Sharma is grateful to the Alexander von Humboldt Foundation (Germany) for financial support during his research stay at Friedrich-Schiller University of Jena.

References

[1] Liedberg B, Nylander C and Sundström I 1983 Surface plasmon resonance for gas detection and biosensing *Sensors Actuators* **4** 299–304
[2] Villuendas F and Pelayo J 1990 Optical fibre device for chemical sensing based on surface plasmon excitation *Sensors Actuators* A **23** 1142–5
[3] Jorgenson R C and Yee S S 1993 A fiber optic chemical sensor based on surface plasmon resonance *Sensors Actuators* B **12** 213–20
[4] Tanahashi E, Iwagishi H and Chang G 2008 Localized surface plasmon resonance sensing properties of photocatalytically prepared Au/TiO_2 films *Mater. Lett.* **62** 2714–6
[5] Kretchmann E 1971 Die Bestimmung optischer konstanten von Metallen durch Anregung von Oberflachenplasmaschwingungen *Z. Phys.* **241** 313–24
[6] Ozdemir S K and Sayan G T 2003 Temperature effects on surface plasmon resonance: design considerations for an optical temperature sensor *J. Light Technol.* **21** 805–14
[7] Chen C W, Lin W C, Liao L S, Lin Z H, Chiang H P, Leung P T, Sijercic E and Tse W S 2007 Optical temperature sensing based on the Goos–Hänchen effect *Appl. Opt.* **46** 5347–51
[8] Sharma A K and Mohr G J 2008 On the performance of surface plasmon resonance based fibre optic sensor with different bimetallic nanoparticle alloy combinations *J. Phys. D: Appl. Phys.* **41** 055106
[9] Ghosh G, Endo M and Iwasaki T 1994 Temperature-dependent Sellmeier coefficients and chromatic dispersions for some optical fiber glasses *J. Light Technol.* **12** 1338–42
[10] Chiang H P, Leung P T and Tse W S 1998 The surface plasmon enhancement effect on adsorbed molecules at elevated temperatures *J. Chem. Phys.* **108** 2659–60
[11] Holstein T 1954 Optical and infrared volume absorptivity of metals *Phys. Rev.* **96** 535–6
[12] McKay J A and Rayne J A 1976 Temperature dependence of the infrared absorptivity of the noble metals *Phys. Rev.* B **13** 673–85
[13] Beach R T and Christy R W 1977 Electron–electron scattering in the intraband optical conductivity of Cu, Ag and Au *Phys. Rev.* B **16** 5277–84
[14] Lawrence W E 1976 Electron–electron scattering in the low-temperature resistivity of the noble metals *Phys. Rev.* B **13** 5316–19
[15] Roy R K, Mandal S K and Pal A K 2003 Effect of interfacial alloying on the surface plasmon resonance of nanocrystalline Au–Ag multilayer thin films *Eur. Phys. J.* B **33** 109–14
[16] Irani G B, Huen T and Wooten F 1971 Optical properties of Ag and α-phase Ag–Al alloys *Phys. Rev.* B **3** 2385–90

[17] Irani G B, Huen T and Wooten F 1972 Optical properties of gold and α-phase gold–aluminum alloys *Phys. Rev.* B **6** 2904–9

[18] Link S, Wang Z L and El-Sayed M A 1999 Alloy formation of gold–silver nanoparticles and the dependence of the plasmon absorption on their composition *J. Phys. Chem.* B **103** 3529–33

[19] Scheibener P, Straub J and Sengers J 1990 Refractive index of water and steam as a function of wavelength, temperature, and density *J. Phys. Chem. Ref. Data* **19** 677–717

[20] Sharma A K and Gupta B D 2006 Fiber optic sensor based on surface plasmon resonance with Ag–Au nanoparticle films *Nanotechnology* **17** 124–31